

Reduced thermal boundary conductance in GaN-based electronic devices introduced by metal bonding layer

Susu Yang^{1,2,§}, Houfu Song^{3,§}, Yan Peng⁴, Lu Zhao³, Yuzhen Tong¹, Feiyu Kang^{3,5,6}, Mingsheng Xu⁷ (✉), Bo Sun^{3,5} (✉), and Xinqiang Wang^{1,2} (✉)

¹ State Key Laboratory for Mesoscopic Physics and Frontiers Science Center for Nano-optoelectronics, School of Physics, Peking University, Beijing 100871, China

² Dongguan Institute of Opto-Electronics, Peking University, Dongguan 523808, China

³ Tsinghua-Berkeley Shenzhen Institute, Tsinghua University, Shenzhen 518055, China

⁴ Institute of Novel Semiconductors and State Key Laboratory of Crystal Material, Shandong University, Jinan 250100, China

⁵ Tsinghua Shenzhen International Graduate School, and Guangdong Provincial Key Laboratory of Thermal Management Engineering & Materials, Tsinghua University, Shenzhen 518055, China

⁶ Laboratory of Advanced Materials, School of Materials Science and Engineering, Tsinghua University, Beijing 100084, China

⁷ Institute of Novel Semiconductors and School of Microelectronics, Shandong University, Jinan 250100, China

[§] Susu Yang and Houfu Song contributed equally to this work.

© Tsinghua University Press and Springer-Verlag GmbH Germany, part of Springer Nature 2021

Received: 24 March 2021 / Revised: 2 June 2021 / Accepted: 6 June 2021

ABSTRACT

Achieving high interface thermal conductance is one of the biggest challenges in the nanoscale heat transport of GaN-based devices such as light emitting diodes (LEDs), and high electron mobility transistors (HEMTs). In this work, we experimentally measured thermal boundary conductance (TBC) at interfaces between GaN and the substrates with AuSn alloy as a commonly-used adhesive layer by time-domain thermoreflectance (TDTR). We find that the TBCs of GaN/Ti/AuSn/Ti/Si, GaN/Ti/AuSn/Ti/SiC, and GaN/Ti/AuSn/Ti/diamond, are 16.5, 14.8, and 13.2 MW·m⁻²·K⁻¹ at room temperature, respectively. Our measured results show that the TBC of GaN/Ti/AuSn/Ti/SiC interface is inferior to the TBC of pristine GaN/SiC interface, due to the large mismatch of phonon modes between AuSn/Ti and substrates, shown as the difference of Debye temperature of two materials. Overall, we measured the TBC at interface between GaN and thermal conductive substrates, and provided a guideline for designing the interface between GaN and substrate at HEMT from a thermal management point of view.

KEYWORDS

GaN, thermal boundary conductance, time-domain thermoreflectance (TDTR), diffuse mismatch model

1 Introduction

Gallium nitride (GaN) is an important wide bandgap semiconductor commonly used for high electron mobility transistors (HEMTs), high power radio frequency (RF) devices, diodes and power electronics because of its high breakdown voltage, high electron mobility and high-switching-frequency [1–5]. However, in these energy-intensive applications, the performance of GaN-based devices is limited by substantial temperature rise due to massive hot spot induced by high power and high frequency, which causes reduced electron mobility, increased gate leakage, and degraded device lifetime [6–8]. In order to efficiently remove heat from hot spot, high thermal conductivity substrates such as Si (~ 140 W·m⁻¹·K⁻¹), SiC (~ 390 W·m⁻¹·K⁻¹) and diamond (~ 2,000 W·m⁻¹·K⁻¹) are used as heat sinks for GaN-based devices [9–17].

For nanoscale and microscale GaN devices, interfaces play a critical rule in impeding heat dissipation. The thermal boundary resistance (TBR) at interface is equivalent to as large as micrometer-thick heat sink's thermal resistance, and cannot be ignored [18–22]. For example, Ziade et al. [23] reported that

the thermal boundary conductance (TBC, which is the reciprocal of TBR) at the interface of GaN/SiC was 230 MW·m⁻²·K⁻¹, which is equivalent to the thermal resistance of 1.7- μ m-thick SiC. It is thus important to understand the TBR of GaN devices for better design of thermal management.

In practical application, solders like AuSn and AuIn are often used as bonding layers to enhance the heat transfer between GaN and substrates [24, 25]. However, as the AuSn alloy has a low Debye temperature and large Debye temperature mismatch with typical substrates such as Si, the overall heat dissipation performance of introducing AuSn adhesion layer is still an open question. Donovan et al. [26] found that the TBC of Au/GaN interface was 57 MW·m⁻²·K⁻¹ at 300 K, which is only one-fourth of that of the GaN/SiC interface, showing that the mismatch of phonon modes between Au and GaN is a concern for thermal transport. Therefore, experimental investigation on heat dissipation performance on GaN-based devices with AuSn adhesion layer is of great importance.

In this paper, we measured the thermal boundary conductance at the interface of GaN and substrates with AuSn/Ti as an adhesion layer. By using time domain thermal-reflectance

(TDTR), the TBCs between AuSn/Ti adhesion layer and Si, SiC, diamond, and GaN were measured as 37.0, 29.5, 23.5, and 31.2 MW·m⁻²·K⁻¹ at room temperature, respectively. We find that the TBC of GaN/Ti/AuSn/Ti/SiC is much lower than the TBC of pristine GaN/SiC interface where GaN was directly grown on SiC substrate, showing that the introduction of AuSn/Ti adhesion layer causes an inefficient heat dissipation at interface. This is understood by the large mismatch of Debye temperature between AuSn/Ti and the substrates. Our work provides an important benchmark for TBC of AuSn/Ti adhesion layer with common substrates, and thus helps improve the thermal design of GaN-based devices.

2 Experimental

2.1 Materials growth

The schematic illustration of the fabrication of samples is shown in Fig. 1(a). The three substrates (Si, SiC, and diamond) and GaN were evaporated with AuSn/Ti on the surface. Si wafer was purchased from Sumco Corporation, while high quality diamond and 4H-SiC substrates were homegrown in Shandong University [27, 28]. The p-type Si(111) and the 4H-SiC(0001) had resistivities of 10 and 10⁸ Ω·cm⁻¹, respectively. Diamond was grown in cubic high-pressure apparatus under high temperature of 1,300–1,500 °C and at a nominal pressure of 5.6 GPa. The surface of substrates was cleaned by ethanol, acetone, and de-ionized water before loading into the vacuum chamber for e-beam evaporation. An adhesion layer of 5-nm-thick Ti was evaporated on the substrate surface under the vacuum of 2 × 10⁻⁶ mbar with a growth rate of 0.2 Å·s⁻¹, followed by e-beam evaporation of AuSn layer (about 100-nm-thick) under the vacuum of 8 × 10⁻⁶ mbar with a growth rate of 10 Å·s⁻¹. The AuSn target material had a high content of Au (80 wt.%) and low content of Sn (20 wt.%), following the application of AuSn solder commonly used in semiconductor industry [29]. The cross-sectional transmission electron microscopy (TEM) images of AuSn/Ti/SiC interface are shown in Figs. 1(b) and 1(c). The thickness of AuSn/Ti layer was measured as 122 nm, which is consistent with the nominal thickness. It can be seen that there is an amorphous Ti layer between the AuSn bonding layer and SiC substrate. The GaN was grown by metal-organic chemical vapor deposition (MOCVD) using a 200-nm-thick nucleation layer on Si(111) substrate with a thickness of ~ 1 mm.

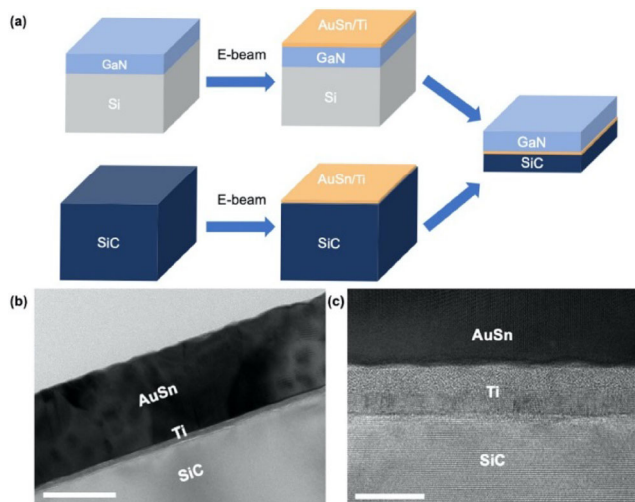


Figure 1 (a) Schematic figure of GaN/SiC interface with introduction of AuSn/Ti bonding. (b) and (c) Cross-sectional TEM images of AuSn/Ti/SiC interface. The scale bar is 100 nm in (b) and 10 nm in (c).

2.2 Thermal conductivity measurement

We used TDTR to characterize the thermal properties of the samples. The fundamental of this method can be found elsewhere [30–33]. In a typical measurement, a periodically modulated pump laser was used to heat the sample, while the time-delayed probe laser beam measured the surface temperature through the change in the reflectance of AuSn, which served as a transducer. The amplitude and phase response of the reflected probe beam was recorded by a lock-in amplifier. The 1/e² radii of the pump and probe beams were both 12 μm at the sample surface. The selection of modulation frequency of the pump has a great impact on the measurement sensitivity to thermal conductance, which affects the measurement uncertainty of TBC. The suitable modulation frequencies of the pump for AuSn/Ti on three substrates (Si, SiC, and diamond) and the GaN sample were 4.6, 10.1, 4.6, and 4.6 MHz, respectively. Samples were loaded into a cryostat (Janis ST-500) with vacuum (~ 10⁻⁶ mbar) at temperature from 100 to 450 K. The TBC and thermal conductivity of substrates were extracted by comparing the experimental data with an analytical solution to the heat diffusion equation of multilayers [30].

3 Results and discussion

The TBCs at AuSn/Ti/GaN and AuSn/Ti/substrate were measured by TDTR, and the equivalent TBC at GaN/substrates with AuSn/Ti bonding layer was calculated.

In the measurement, the TBC of AuSn/Ti/substrate is defined as one unknown parameter for the fitting. Considering that the thermal conductance at metal/metal interface is at ~ GW·m⁻²·K⁻¹ [34, 35], and the Ti layer has a thickness of 5 nm, the contribution of TBC_{AuSn/Ti} and thermal conductivity of Ti λ_{Ti} to the overall TBC of AuSn/Ti/substrate interface is neglectable. To show the validity of TDTR measurement, the measured data and best fitting of Si, SiC, GaN, and diamond are shown in Fig. 2, which shows the fitted curves are in good agreement with experimental data.

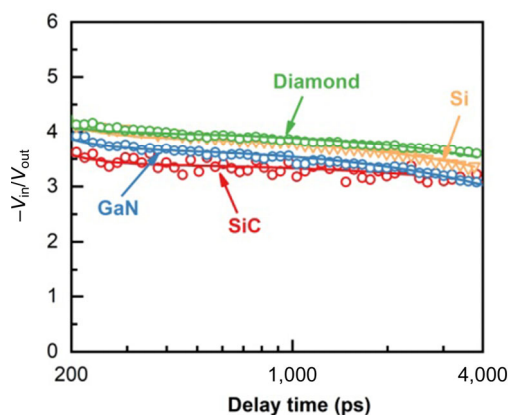


Figure 2 Experimental data (open circles) and best fitting (solid lines) of TDTR measured results.

To further check the reliability of the parameter setup of this thermal model, we performed the sensitivity analysis and present the result in Fig. 3. The sensitivity S_α to any parameter α in our thermal model is calculated as [29]

$$S_\alpha = \frac{\partial \ln(-V_{in}/V_{out})}{\partial \ln \alpha} \quad (1)$$

where S_α is the sensitivity to parameter α ; $-V_{in}/V_{out}$ is the TDTR signal, and α is the parameter we are interested in. High sensitivity S_α indicates that the thermal model is suitable

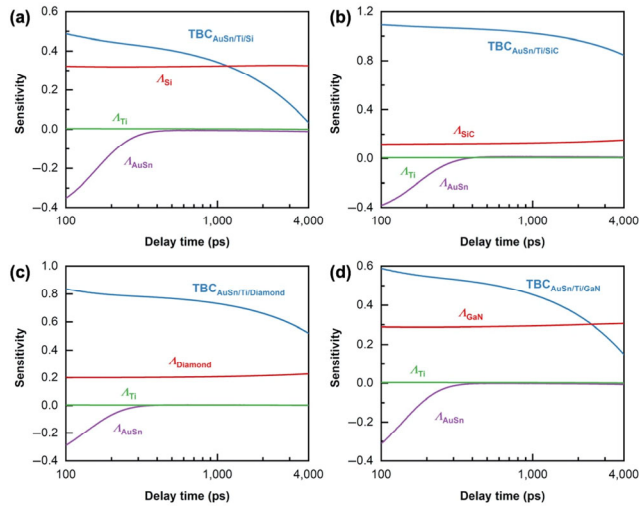


Figure 3 The sensitivity of TDTR measurement to AuSn thermal conductivity λ_{AuSn} , Ti thermal conductivity λ_{Ti} , TBC at interface, and substrate thermal conductivity λ for (a) Si, (b) SiC, (c) diamond, and (d) GaN samples.

for measurement of parameter α . Two notable features can be seen from Fig. 3. First, the sensitivity to TBC of all the samples is larger than 0.2 in most of delay time, showing that the thermal model is sensitive enough for TBC measurement. Second, the sensitivity to TBC (> 0.4 for all samples at 100 ps) is much higher than the sensitivity to substrate thermal conductivity, indicating that the thermal boundary resistance at AuSn/Ti/substrate interface is dominant when heat flows across the interface. The sensitivity to substrate thermal conductivity increases at longer delay time, which is physically intuitive as the heat is diffused into the substrate.

The parameters used to calculate sensitivities are given in Table 1, where C_v is volumetric heat capacity; Λ_{\perp} is thermal conductivity at cross-plane direction, and d is thickness. As the $1/e^2$ radius of the laser spot size is 12 μm , large enough to ensure one-dimensional heat flow approximation at the cross-plane direction, the anisotropic thermal conductivity of the substrate is neglected [36].

Specifically, the thickness of AuSn alloy is crucial to measurement results, so a careful calculation of thickness was carried out using picoacoustics (Fig. 4) [42] and the thickness of AuSn/Ti is determined to be 100 to 120 nm, which is consistent with the thickness in cross-sectional TEM images. By summing up the error introduced by each parameter using calculated sensitivity, the uncertainty of measured TBCs is deduced as 4%–10% for all samples.

The prediction of TBC is achieved by applying diffuse mismatch model (DMM) [43]. In this model, only elastic phonon scattering is considered, and a phonon with frequency ω can only transmit energy across the interface with another phonon with the same frequency ω . Assuming a Debye approximation of phonon dispersion relationship, the phonon transmission probability $\alpha_A(\omega)$ can be written as [43]

Table 1 Parameters used to calculate the sensitivity at 300 K.

Material	C_v ($\text{MJ}\cdot\text{m}^{-3}\cdot\text{K}^{-1}$)	Λ_{\perp} ($\text{W}\cdot\text{m}^{-1}\cdot\text{K}^{-1}$)	d (nm)	Ref.
AuSn	2.16	58	104–116	[37]
Ti	2.37	22	5	[38]
SiC	2.08	390	Bulk	[39]
Si	1.60	140	Bulk	[40]
Diamond	1.81	1,100	Bulk	[41]
GaN	2.61	200	Bulk	[39]

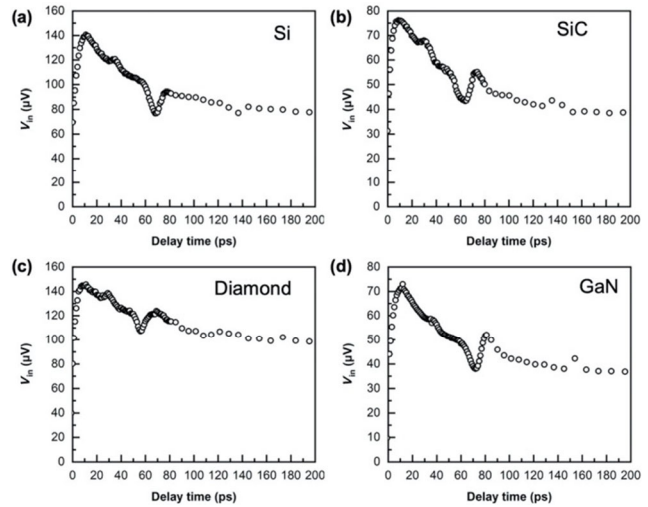


Figure 4 The picoacoustics from TDTR measurement of (a) Si, (b) SiC, (c) diamond, and (d) GaN samples.

$$\alpha_A(\omega) = \frac{\sum_j v_B^{-2}}{\sum_j v_A^{-2} + \sum_j v_B^{-2}} \quad (2)$$

where v is phonon group velocity; subscripts A and B refers to materials at one and the other side of interface, respectively, and j is the branch of phonons. In this way, TBC is given by [43]

$$\text{TBC} = \frac{1}{4} \sum_j \int_0^{\omega_{A,j}^{\text{Debye}}} D_{A,j}(\omega) \frac{\partial}{\partial T} f(\omega, T) \hbar \omega \cdot v_{A,j} \cdot \alpha_A(\omega) d\omega \quad (3)$$

where D is the phonon density of states; f is Bose-Einstein distribution; v is phonon group velocity; $\omega_{A,j}^{\text{Debye}}$ is the Debye frequency of phonon mode j in material A. The parameters used for calculation are listed in Table 2. The measured data and calculated TBC as a function of temperature are concluded in Fig. 5. The measured TBCs for AuSn/Ti/Si, AuSn/Ti/SiC, AuSn/Ti/diamond, and AuSn/Ti/GaN interface are 37.0 ± 2.2 , 29.5 ± 1.9 , 23.5 ± 1.7 , and 31.2 ± 2.7 $\text{MW}\cdot\text{m}^{-2}\cdot\text{K}^{-1}$ at 300 K. The difference of TBC is caused by the mismatch of phonon dispersion between Ti and Si, SiC, GaN, and diamond substrates [44], which can be seen from the difference of Debye temperature (Table 2).

The TBC predicted by DMM shows similarity in temperature dependency with the measured data: The thermal conductance increases as the temperature rises due to the increasing number of phonons participating in heat transport at interfaces, which is the basics for DMM and other Landauer-based theories that phonons are viewed as quasi-particles [46]. However, the measured TBC is lower than the DMM calculated value by 50% to 90%, showing that the defects are critical for interface heat transfer [47].

Table 2 Thermal properties used to calculate the DMM using Eq. (3), including acoustic longitudinal and transverse speeds (v_l and v_t) of sound and Debye temperature T_D of materials

Material	v_l ($\text{m}\cdot\text{s}^{-1}$)	v_t ($\text{m}\cdot\text{s}^{-1}$)	T_D (K)	Ref.
AuSn	1,292	3,233	—	[37]
Si	5,332	8,970	645	[44]
SiC	7,100	13,100	1,300	[23]
Ti	3,125	6,070	270	[45]
Diamond	12,800	17,500	2,250	[23]
GaN	4,130	8,040	600	[39]
AlN	6,220	10,970	1,150	[39]

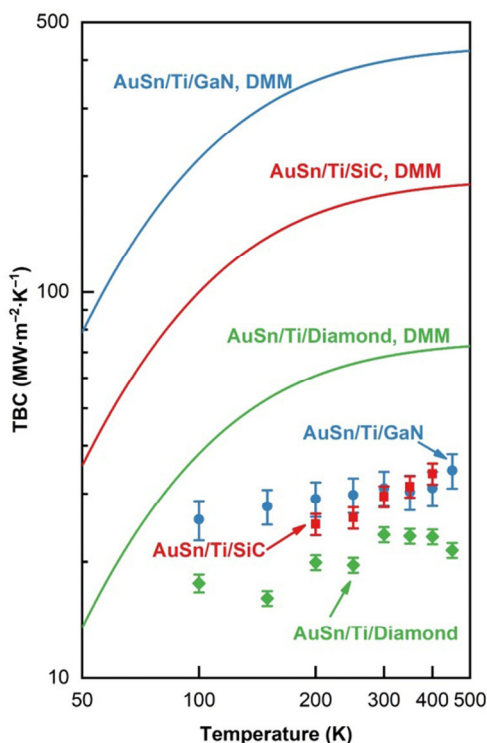


Figure 5 Measured and calculated results by DMM at interface between AuSn/Ti and substrates. The measured results are shown in solid symbols, and DMM prediction values are shown in lines.

As AuSn is a commonly used adhesive layer for GaN-based devices, we used the measured result to calculate the TBC at GaN/substrate interface with Ti/AuSn/Ti as bonding layer. The TBC of GaN/Ti/AuSn/Ti/SiC was calculated by Fourier's Law using TBC of AuSn/Ti/GaN and TBC of AuSn/Ti/SiC. In the thermal model, the heat is conducted in a layered structure from GaN to SiC, and the thermal resistance can be divided into five parts: GaN/Ti, Ti, AuSn, Ti, and Ti/SiC. The thicknesses of Ti and AuSn were set as 5 and 40 nm, respectively, and the total thermal resistance was calculated, as shown in Table 3. Based on the calculation, when the bonding layer is Ti (5 nm)/AuSn (40 nm)/Ti (5 nm), the TBCs are 16.5, 14.8, and 13.2 $\text{MW}\cdot\text{m}^{-2}\cdot\text{K}^{-1}$ for GaN on Si, SiC, and diamond, respectively. Noting that this value is significantly lower than the TBC of pristine GaN/SiC interface, the introduction of AuSn/Ti bonding layer is negative in the overall heat transfer performance.

Table 3 Calculation of TBC at GaN/Ti/AuSn/Ti/SiC interface

Layer	GaN/Ti	Ti	AuSn	Ti	Ti/SiC
Thermal conductivity ($\text{W}\cdot\text{m}^{-1}\cdot\text{K}^{-1}$)	0.0312	17	58	17	0.0295
Thickness (nm)	1	5	40	5	1
Thermal resistance ($\text{m}^2\cdot\text{K}\cdot\text{W}^{-1}$)	3.2×10^{-8}	2.9×10^{-10}	6.9×10^{-10}	2.9×10^{-10}	3.4×10^{-8}
Total thermal resistance ($\text{m}^2\cdot\text{K}\cdot\text{W}^{-1}$)	6.8×10^{-8}				
Total thermal conductance ($\text{MW}\cdot\text{m}^{-2}\cdot\text{K}^{-1}$)	14.8				

4 Conclusion

In this work, we fabricated a AuSn/Ti layer on Si, SiC, diamond substrates, and GaN-based devices. The TBC of GaN on substrates with AuSn/Ti bonding layer was measured by TDTR method. The total TBCs between GaN-HEMT and the substrates

(Si or SiC or diamond) with a bonding layer of Ti (5 nm)/AuSn (40 nm)/Ti (5 nm) are 16.5, 14.8, and 13.2 $\text{MW}\cdot\text{m}^{-2}\cdot\text{K}^{-1}$, respectively, substantially lower than the thermal conductance of GaN/SiC interface. The reduction on thermal conductance is attributed to the mismatch of phonon frequencies across the interface. Our work provides a guiding significance that the introduction of metal bonding layer is not naturally beneficial for heat conduction, the overall performance is limited by phonon dispersion mismatch at the interface.

Acknowledgements

This work was supported by the National Natural Science Foundation of China (No. 12004211), the Guangdong Natural Science Foundation (No. 2019A1515010868), the Guangdong Key Research and Development Program (No. 2019B010132001), and Shenzhen Peacock Program. This work was also supported by Beijing Outstanding Young Scientist Program (No. BJJWZYJH0120191000103), and the Major Science and Technology Innovation Project of Shandong Province (No. 2019JZZY010210).

References

- Asif Khan, M.; Bhattarai, A.; Kuznia, J.; Olson, D. High electron mobility transistor based on a GaN-Al_xGa_{1-x}N heterojunction. *Appl. Phys. Lett.* **1993**, *63*, 1214–1215.
- Morkoç, H.; Strite, S.; Gao, G. B.; Lin, M. E.; Sverdlov, B.; Burns, M. Large-band-gap SiC, III-V nitride, and II-VI ZnSe-based semiconductor device technologies. *J. Appl. Phys.* **1994**, *76*, 1363–1398.
- Tsao, J. Y.; Chowdhury, S.; Hollis, M. A.; Jena, D.; Johnson, N. M.; Jones, K. A.; Kaplar, R. J.; Rajan, S.; Van de Walle, C. G.; Bellotti, E. et al. Ultrawide-bandgap semiconductors: Research opportunities and challenges. *Adv. Electron. Mater.* **2018**, *4*, 1600501.
- Oka, T.; Nozawa, T. AlGaIn/GaN recessed MIS-gate HFET with high-threshold-voltage normally-off operation for power electronics applications. *IEEE Electron Device Lett.* **2008**, *29*, 668–670.
- Lester, S. D.; Ponce, F. A.; Craford, M. G.; Steigerwald, D. A. High dislocation densities in high efficiency GaN-based light-emitting diodes. *Appl. Phys. Lett.* **1995**, *66*, 1249–1251.
- Xu, J. F.; Yin, W. Y.; Mao, J. F. Transient thermal analysis of GaN heterojunction transistors (HFETs) for high-power applications. *IEEE Microw. Wirel. Compon. Lett.* **2007**, *17*, 55–57.
- Meneghesso, G.; Verzellesi, G.; Danesin, F.; Rampazzo, F.; Zanon, F.; Tazzoli, A.; Meneghini, M.; Zanoni, E. Reliability of GaN high-electron-mobility transistors: State of the art and perspectives. *IEEE Trans. Device Mater. Reliab.* **2008**, *8*, 332–343.
- Sun, B.; Haunschild, G.; Polanco, C.; Ju, J.; Lindsay, L.; Koblmüller, G.; Koh, Y. K. Dislocation-induced thermal transport anisotropy in single-crystal group-III nitride films. *Nat. Mater.* **2019**, *18*, 136–140.
- Wei, L. H.; Kuo, P. K.; Thomas, R. L.; Anthony, T. R.; Banholzer, W. F. Thermal conductivity of isotopically modified single crystal diamond. *Phys. Rev. Lett.* **1993**, *70*, 3764–3767.
- Turin, V. O.; Balandin, A. A. Performance degradation of GaN field-effect transistors due to thermal boundary resistance at GaN/substrate interface. *Electron. Lett.* **2004**, *40*, 81–83.
- Sarua, A.; Ji, H. F.; Kuball, M.; Uren, M. J.; Martin, T.; Hilton, K. P.; Balmer, R. S. Integrated micro-Raman/infrared thermography probe for monitoring of self-heating in AlGaIn/GaN transistor structures. *IEEE Trans. Electron Devices* **2006**, *53*, 2438–2447.
- Mohanty, S. K.; Chen, Y. Y.; Yeh, P. H.; Horng, R. H. Thermal Management of GaN-on-Si high electron mobility transistor by copper filled micro-trench structure. *Sci. Rep.* **2019**, *9*, 19691.
- Slack, G. A. Thermal conductivity of pure and impure silicon, silicon carbide, and diamond. *J. Appl. Phys.* **1964**, *35*, 3460–3466.
- Qian, X.; Jiang, P. Q.; Yang, R. G. Anisotropic thermal conductivity of 4H and 6H silicon carbide measured using time-domain thermoreflectance. *Mater. Today Phys.* **2017**, *3*, 70–75.

- [15] Wei, R. S.; Song, S.; Yang, K.; Cui, Y. X.; Peng, Y.; Chen, X. F.; Hu, X. B.; Xu, X. G. Thermal conductivity of 4H-SiC single crystals. *J. Appl. Phys.* **2013**, *113*, 053503.
- [16] Protik, N. H.; Katre, A.; Lindsay, L.; Carrete, J.; Mingo, N.; Broido, D. Phonon thermal transport in 2H, 4H and 6H silicon carbide from first principles. *Mater. Today Phys.* **2017**, *1*, 31–38.
- [17] Zheng, Q. Y.; Li, C. H.; Rai, A.; Leach, J. H.; Broido, D.; Cahill, D. G. Thermal conductivity of GaN, ⁷¹GaN, and SiC from 150 K to 850 K. *Phys. Rev. Mater.* **2019**, *3*, 014601.
- [18] Cheng, Z.; Yates, L.; Shi, J. J.; Tadjer, M. J.; Hobart, K. D.; Graham, S. Thermal conductance across β -Ga₂O₃-diamond van der Waals heterogeneous interfaces. *APL Mater.* **2019**, *7*, 031118.
- [19] Gaskins, J. T.; Kotsolis, G.; Giri, A.; Ju, S. H.; Rohskopf, A.; Wang, Y. K.; Bai, T. Y.; Sachet, E.; Shelton, C. T.; Liu, Z. Y. et al. Thermal boundary conductance across heteroepitaxial ZnO/GaN interfaces: Assessment of the phonon gas model. *Nano Lett.* **2018**, *18*, 7469–7477.
- [20] Ju, J.; Sun, B.; Haunschild, G.; Loitsch, B.; Stoib, B.; Brandt, M. S.; Stutzmann, M.; Koh, Y. K.; Koblmüller, G. Thermoelectric properties of In-rich InGaN and InN/InGaN superlattices. *AIP Adv.* **2016**, *6*, 045216.
- [21] Mu, F. W.; Cheng, Z.; Shi, J. J.; Shin, S.; Xu, B.; Shiomi, J.; Graham, S.; Suga, T. High thermal boundary conductance across bonded heterogeneous GaN–SiC interfaces. *ACS Appl. Mater. Interfaces* **2019**, *11*, 33428–33434.
- [22] Sun, B.; Gu, X. K.; Zeng, Q. S.; Huang, X.; Yan, Y. X.; Liu, Z.; Yang, R. G.; Koh, Y. K. Temperature dependence of anisotropic thermal-conductivity tensor of bulk black phosphorus. *Adv. Mater.* **2017**, *29*, 1603297.
- [23] Ziade, E.; Yang, J.; Brummer, G.; Nothorn, D.; Moustakas, T.; Schmidt, A. J. Thermal transport through GaN–SiC interfaces from 300 to 600 K. *Appl. Phys. Lett.* **2015**, *107*, 091605.
- [24] Cho, J.; Li, Z. J.; Asheghi, M.; Goodson, K. E. Near-junction thermal management: Thermal conduction in gallium nitride composite substrates. *Annu. Rev. Heat Transfer* **2015**, *18*, 7–45.
- [25] Ji, H. F.; Das, J.; Germain, M.; Kuball, M. Laser lift-off transfer of AlGaIn/GaN HEMTs from sapphire onto Si: A thermal perspective. *Solid State Electron.* **2009**, *53*, 526–529.
- [26] Donovan, B. F.; Szejewski, C. J.; Duda, J. C.; Cheaito, R.; Gaskins, J. T.; Peter Yang, C. Y.; Constantin, C.; Jones, R. E.; Hopkins, P. E. Thermal boundary conductance across metal-gallium nitride interfaces from 80 to 450 K. *Appl. Phys. Lett.* **2014**, *105*, 203502.
- [27] Xie, X. J.; Wang, X. W.; Peng, Y.; Cui, Y. X.; Chen, X. F.; Hu, X. B.; Xu, X. G.; Yu, P.; Wang, R. Q. Synthesis and characterization of high quality {100} diamond single crystal. *J. Mater. Sci. Mater. Electron.* **2017**, *28*, 9813–9819.
- [28] Xie, X. J.; Hu, X. B.; Chen, X. F.; Liu, F. F.; Yang, X. L.; Xu, X. G.; Wang, H.; Li, J.; Yu, P.; Wang, R. Q. Characterization of the three-dimensional residual stress distribution in SiC bulk crystals by neutron diffraction. *CrystEngComm* **2017**, *19*, 6527–6532.
- [29] Zhou, T.; Bobal, T.; Oud, M.; Songliang, J. Au/Sn solder alloy and its applications in electronics packaging. *Coining Inc* **1999**.
- [30] Cahill, D. G. Analysis of heat flow in layered structures for time-domain thermoreflectance. *Rev. Sci. Instrum.* **2004**, *75*, 5119–5122.
- [31] Sun, B.; Koh, Y. K. Understanding and eliminating artifact signals from diffusely scattered pump beam in measurements of rough samples by time-domain thermoreflectance (TDTR). *Rev. Sci. Instrum.* **2016**, *87*, 064901.
- [32] Schmidt, A. J.; Chen, X. Y.; Chen, G. Pulse accumulation, radial heat conduction, and anisotropic thermal conductivity in pump-probe transient thermoreflectance. *Rev. Sci. Instrum.* **2008**, *79*, 114902.
- [33] Feser, J. P.; Liu, J.; Cahill, D. G. Pump-probe measurements of the thermal conductivity tensor for materials lacking in-plane symmetry. *Rev. Sci. Instrum.* **2014**, *85*, 104903.
- [34] Gundrum, B. C.; Cahill, D. G.; Averback, R. S. Thermal conductance of metal-metal interfaces. *Phys. Rev. B* **2005**, *72*, 245426.
- [35] Wilson, R. B.; Cahill, D. G. Experimental validation of the interfacial form of the Wiedemann-Franz law. *Phys. Rev. Lett.* **2012**, *108*, 255901.
- [36] Feser, J. P.; Cahill, D. G. Probing anisotropic heat transport using time-domain thermoreflectance with offset laser spots. *Rev. Sci. Instrum.* **2012**, *83*, 104901.
- [37] King, J. A. *Materials Handbook for Hybrid Microelectronics*; Artech House: Boston, 1988.
- [38] Desai, P. D. Thermodynamic properties of titanium. *Int. J. Thermophys.* **1987**, *8*, 781–794.
- [39] Levinshtein, M. E.; Rumyantsev, S. L.; Shur, M. S. *Properties of Advanced Semiconductor Materials: GaN, AlN, InN, BN, SiC, SiGe*; Wiley: New York, 2001.
- [40] Minnich, A. J.; Johnson, J. A.; Schmidt, A. J.; Esfarjani, K.; Dresselhaus, M. S.; Nelson, K. A.; Chen, G. Thermal conductivity spectroscopy technique to measure phonon mean free paths. *Phys. Rev. Lett.* **2011**, *107*, 095901.
- [41] DeSorbo, W. Specific heat of diamond at low temperatures. *J. Chem. Phys.* **1953**, *21*, 876–880.
- [42] Thomsen, C.; Grahn, H. T.; Maris, H. J.; Tauc, J. Surface generation and detection of phonons by picosecond light pulses. *Phys. Rev. B* **1986**, *34*, 4129–4138.
- [43] Swartz, E. T.; Pohl, R. O. Thermal boundary resistance. *Rev. Mod. Phys.* **1989**, *61*, 605–668.
- [44] Hopkins, P. E.; Norris, P. M.; Stevens, R. J. Influence of inelastic scattering at metal-dielectric interfaces. *J. Heat Transfer* **2008**, *130*, 022401.
- [45] Lide, D. R. *CRC Handbook of Chemistry and Physics*; CRC Press: Boca Raton, 2004.
- [46] Imry, Y.; Landauer, R. Conductance viewed as transmission. *Rev. Mod. Phys.* **1999**, *71*, S306–S312.
- [47] Hopkins, P. E.; Phinney, L. M.; Serrano, J. R.; Beechem, T. E. Effects of surface roughness and oxide layer on the thermal boundary conductance at aluminum/silicon interfaces. *Phys. Rev. B* **2010**, *82*, 085307.